References

[1] Ericsson, L.-E., Woods, P., and Chavez, J. N., "A mechanism for self-excited oscillations of 'Hammerhead' and other blunt-nose missiles," *Proceedings of the 6th Symposium on Ballistic Missile and Space Technology* (Academic Press, New York, 1961), Vol. IV, pp. 68–88.

[2] Woods, P. and Ericsson, L.-E., "Aeroelastic considerations in a slender blunt-nose, multistage rocket," Aerospace Eng. 21, 42–51 (May 1962).

[3] Reding, J. P. and Ericsson, L.-E., "Static loads on the Saturn I-Apollo launch vehicle," Lockheed Missiles and Space Company, LMSC TM 53-40-143 (LMSC-803185), Contract No. NAS 8-5338 (November 1962).

[4] Norburg, J. F. and Crabtree, L. F., "A simplified model of the incompressible flow past two-dimensional airfoils with a long bubble type of flow separation," Royal Aircraft Establishment, RAE TN Aero 2352 (June 1955).

[5] Kuehn, D. M., "Turbulent boundary-layer separation induced by flares on cylinders at zero angle of attack," NASA Ames Research Center, NASA TR R-117 (1961).

[6] Kistler, A. L. and Chen, W. S., "The fluctuating pressure field in a supersonic turbulent boundary layer," Jet Propulsion Laboratory, California Institute of Technology, TR 32-277 (August 1962).

[7] Bisplinghoff, R. L., Ashley, H., and Halfman, R. L., *Aeroelasticity* (Addison-Wesley Publishing Co., Inc., Cambridge, Mass., 1955).

[8] Rainey, G. "Progress on the launch vehicle buffeting problem," *5th Annual Structures and Materials Conference of the American Institute of Aeronautics and Astronautics* (AIAA, New York, 1964), pp. 163–177.

[9] Cole, H., Jr., Robinson, R., and Gambucci, B., "Buffeting response of the Apollo partial mode model at subsonic and supersonic Mach numbers," NASA Ames Research Center, NASA TN-D 2689 (February 1965).

JULY-AUG. 1965 J. SPACECRAFT VOL. 2, NO. 4

Laminar Boundary-Layer Growth on Slightly Blunted Cones at Hypersonic Speeds

R. E. WILSON*
U. S. Naval Ordnance Laboratory, White Oak, Silver Spring, Md.

A momentum-integral method is given for calculating the subject boundary-layer growth for the zero-angle-of-attack case. Available flat-plate boundary-layer results permit calculations for slightly blunted cones for wide ranges of hypersonic Mach number and surface temperature. Although perfect gas data are used, real gas data for equilibrium air can be introduced. Numerical results are presented for a slender cone. The results show that slight blunting greatly affects conditions at the outer edge of the boundary layer. The Mach number is markedly decreased at long distances from the tip. This is accompanied by an increase in temperature and a decrease in unit Reynolds number. The distributions through the boundary layer of parameters such as temperature and electron density will be affected. Both local skin friction and heat transfer are significantly reduced by slight blunting.

Nomenclature

a = shock radius of curvature
b = tip radius of curvature
c_f = $2\tau_w/\tau_1 u_1^2$ = local skin-friction coefficient
c_{fc} = $2\tau_w/\rho_c u_c^2$
F_1 = function defined by Eq. (13)
F_2 = function defined by Eq. (16)
H = δ^*/θ = boundary-layer shape parameter
M = Mach number
P = pressure
Pr = Prandtl number
q = local heat-transfer rate
r = local cone radius
r_s = radius of streamtube in undisturbed flow
R = Reynolds number, $R_c = \rho_c u_c x/\mu_c$, $R_{\theta c} = \rho_c u_c \theta/\mu_c$, $R_{bc} = \rho_c u_c b/\mu_c$, $R_{\theta 1} = \rho_1 u_1 \theta/\mu_1$
St = local Stanton number
T = temperature
x = distance along cone surface measured from apex
y = distance normal to surface
γ = ratio of specific heats
δ = boundary-layer thickness
$\delta^* = \int_0^\delta \left(1 - \frac{\rho u}{\rho_1 u_1}\right) dy$ = boundary-layer displacement thickness
$\theta = \int_0^\delta \left(\frac{\rho u}{\rho_1 u_1}\right)\left(1 - \frac{u}{u_1}\right) dy$ = boundary-layer momentum thickness
μ = absolute viscosity
ξ = $R_c R_{\theta c}/R_{bc}^2$
ρ = density
σ = cone half-angle
τ = shear stress
ω = shock-wave angle for sharp cone
ω_s = local shock-wave angle for blunt cone

Subscripts

c = conditions at the outer edge of the boundary layer on a sharp cone
w = conditions at the wall
l = local conditions at the outer edge of the boundary layer
∞ = freestream conditions
T = stagnation conditions

Superscripts

$'$ = reference value
0 = sharp-cone values

Received May 13, 1964; revision received September 10, 1964.

* Associate Technical Director, Aeroballistics. Associate Fellow Member AIAA.

Introduction

SUPERSONIC experiments have shown that slight blunting of the leading edge of a surface or the tip of a cone can cause a significant downstream movement of transition to turbulence.[1–5] This effect is associated with the decrease in unit Reynolds number at the outer edge of the boundary layer. Moeckel[6] estimated the bluntness required for maximum downstream movement of transition. The bluntness was chosen so that transition occurred just before the boundary layer began "swallowing" the shear layer or variable entropy layer behind the curved shock. For smaller bluntness than this, transition to turbulence can occur at some point during the swallowing process. A calculation of the laminar boundary-layer growth during the swallowing process is therefore of interest in connection with transition.

In calculating conditions at the outer edge of the boundary layer, streamlines passing through the curved shock must be identified as they enter the boundary layer. The streamlines are identified by relating the mass flow through a streamtube ahead of the shock to the flow in the boundary layer at some point along the body. Zakkay and Krause[7] give a method similar to that used in the present paper for identifying the streamlines. The method of Ref. 7 assumes local boundary-layer similarity and makes use of a mass flow function given by Lees.[8] This function includes a parameter giving the boundary-layer growth along the body. In the present paper, the growth along the body is obtained from the boundary-layer momentum-integral equation. In addition, the shock-wave shapes assumed here and in Ref. 7 are somewhat different. Calculations are given here for the effect of blunting on skin friction and heat transfer as well as on the conditions at the outer edge of the boundary layer.

Theoretical Results

The equations for computing the boundary-layer growth are derived using the coordinate system given in Fig. 1.

Momentum-Integral Equation

The boundary-layer momentum-integral equation for the case of an axisymmetric body is

$$\frac{d\theta}{dx} - \frac{\delta}{\rho_1 u_1^2}\frac{dP}{dx} + \frac{\theta}{\rho_1 u_1^2}\frac{d(\rho_1 u_1^2)}{dx} - \frac{1}{u_1}\frac{du_1}{dx}\int_0^\delta \frac{\rho u}{\rho_1 u_1}\,dy + \frac{\theta}{r}\frac{dr}{dx} = \frac{c_f}{2} - \frac{\tau_1}{\rho_1 u_1^2} \quad (1)$$

In deriving Eq. (1), it is assumed that the boundary layer is thin and that the velocity gradient du/dy at the outer edge of the boundary layer is not necessarily zero.

To simplify Eq. (1) for the case of a slightly blunted cone, assume 1) a constant pressure on the conical surface equal to the inviscid sharp-cone pressure, 2) a thermally and calorifically perfect gas, 3) adiabatic flow outside the boundary layer, and 4) $\tau_1/\rho_1 u_1^2 \ll c_f/2$. With these assumptions, the momentum equation becomes

$$\frac{d\theta}{dx} + \frac{2\theta}{M_1}\left\{1 - \frac{[(\delta/\theta) - H]}{2 + (\gamma - 1)M_1^2}\right\}\frac{dM_1}{dx} + \frac{\theta}{r}\frac{dr}{dx} = \frac{c_f}{2} \quad (2)$$

Note that, for axisymmetric bodies with varying Mach number but isentropic flow outside the boundary layer, the momentum equation is identical to Eq. (2) if the difference $(\delta/\theta) - H$ is replaced by $\gamma M_1^2 - H$. To integrate Eq. (2), it is necessary to obtain expressions for the boundary-layer parameters (c_f, δ/θ, H) and for the Mach number gradient (dM_1/dx).

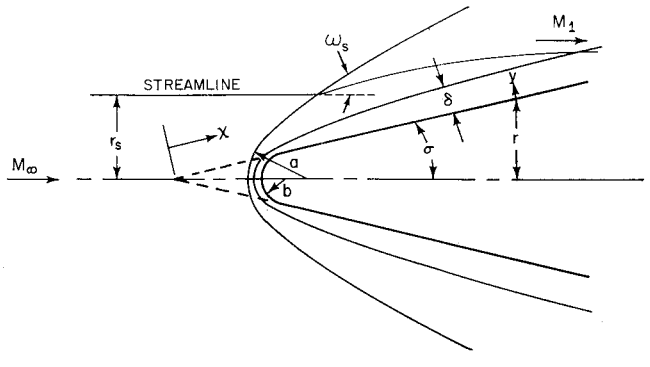

Fig. 1 Coordinate system.

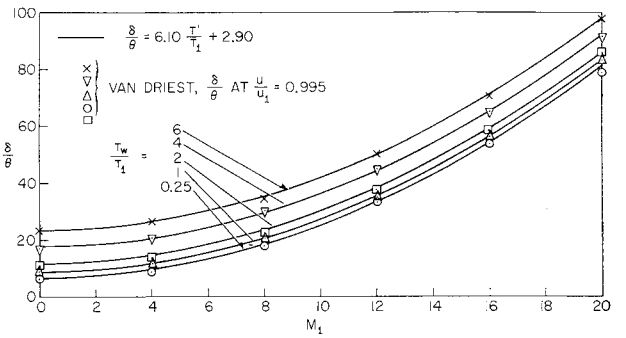

Fig. 2 Flat-plate boundary-layer thickness, $Pr = 0.75$, $\gamma = 1.4$, $T_1 = 392.4°R$.

Boundary-Layer Parameters

The expressions for c_f, δ/θ, and H will be taken from the flat-plate case and evaluated at the local flow conditions at each point along the body. From the well-known Mangler transformation, these expressions apply exactly to the case of a sharp cone. They are assumed to be reasonable approximations for slightly blunted cones. Using Rubesin and Johnson's T' method,[9] the local skin-friction coefficient in terms of the momentum-thickness Reynolds number is

$$c_f = 2\tau_w/\rho_1 u_1^2 = 0.441 T_1 \mu'/T' \mu_1 R_{\theta 1} \quad (3)$$

Reference 10 gives an expression for T'/T_1 which depends on the Prandtl number. For $Pr = 0.75$,

$$T'/T_1 = 1 + 0.076(\gamma - 1)M_1^2 + 0.481[(T_w/T_1) - 1] \quad (4)$$

The ratio μ'/μ_1 in Eq. (3) can be computed from Sutherland's viscosity law. For the case of a perfect gas and adiabatic flow outside the boundary layer, values of T_1 can of course be computed from M_1 and $T_{T\infty}$.

Expressions for δ/θ and H can be obtained by making use of Van Driest's graphs (numerical solutions to the flat-plate laminar boundary-layer equations).[11] Using this information, values of δ/θ and H have been calculated and plotted on Figs. 2 and 3, respectively. It has been found that

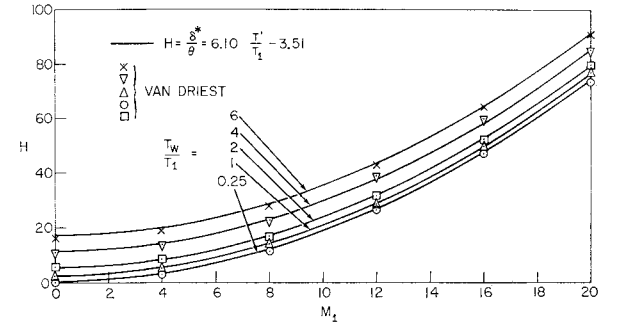

Fig. 3 Flat-plate boundary-layer shape parameter, $Pr = 0.75$, $\gamma = 1.4$, $T_1 = 392.4°R$.

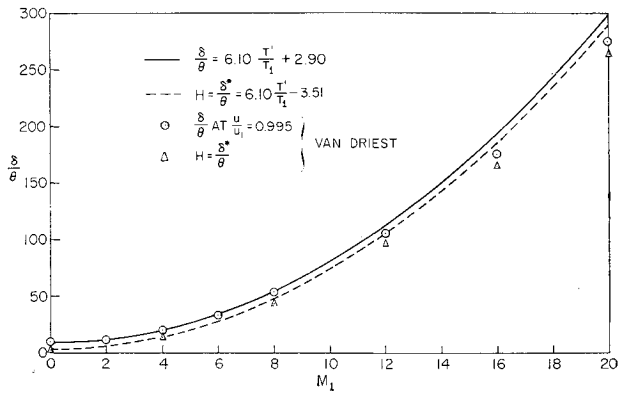

Fig. 4 Flat-plate boundary-layer thickness and shape parameter zero heat transfer, $Pr = 0.75$, $\gamma = 1.4$, $T_1 = 392.4°R$.

δ/θ and H can be approximated by

$$\delta/\theta = 6.10(T'/T_1) + 2.90 \tag{5}$$

$$H = 6.10(T'/T_1) - 3.51 \tag{6}$$

where T'/T_1 is given by Eq. (4). Figures 2 and 3 demonstrate that Eqs. (5) and (6) are excellent fits to the values calculated from Ref. 11 for $0 \leq M_1 \leq 20$ and $0.25 \leq (T_w/T_1) \leq 6.0$. Substituting the T'/T_1 expression for $Pr = 1$ from Ref. 10, Eqs. (5) and (6) can be put in the same form as, and are in reasonable agreement with, analytic expressions for δ/θ and H given in Ref. 12 for $Pr = 1$ and a linear relation between viscosity and temperature. This gives additional confidence in Eqs. (5) and (6).

The difference $(\delta/\theta) - H$ appears in Eq. (2) and also in equations that follow. Equations (5) and (6) yield the convenient result

$$(\delta/\theta) - H = \text{const} = 6.41 \tag{7}$$

Since the Ref. 11 results used to calculate δ/θ and H are in graphical form, the accuracy of the values is difficult to determine. This leads to an uncertainty in the accuracy of the difference $(\delta/\theta) - H$. However, the conclusion that the difference is constant seems valid. Values calculated from Ref. 11 give the difference of 6.41 with an rms deviation of only 10%. This result holds for $0 \leq M_1 \leq 20$ and $0.25 \leq T_w/T_1 \leq 6.0$ with no discernible trend in the deviations.

In addition to the results discussed previously, the case of zero heat transfer is investigated in Ref. 11 for $0 \leq M_1 \leq 20$. For completeness, δ/θ and H for zero heat transfer from Eqs. (5) and (6) are compared in Fig. 4 with values calculated from Ref. 11. The agreement is not as good as that in Figs. 2 and 3, particularly at $M_1 > 8$, but the zero heat-transfer case is of no practical interest for free flight at high M_1 anyway.

Continuity Considerations

To obtain an expression for M_1 and dM_1/dx to be used in the integration of Eq. (2), it is necessary to derive two relations between M_1 and the local shock-wave angle ω_s. The first relation is derived from continuity considerations. For thin boundary layers, the mass flow through a streamtube of radius r_s and the flow in the boundary layer are related by (see Fig. 1)

$$\rho_\infty u_\infty \pi r_s^2 = 2\pi r \int_0^\delta \rho u dy \tag{8}$$

To introduce ω_s, the wave shape is needed. For exact results, experimental data can be used or elaborate flow calculations carried out. For the present work, the shock is assumed to be a hyperbola, as suggested in Ref. 13, and ω_s approaches the sharp-cone value ω as $r_s \to \infty$. Reference 14 gives an expression for the shock radius of curvature a at $r_s = 0$. The values of ω and a define the shape of the hyperbola

$$a^2/r_s^2 = \tan^2\omega_s - \tan^2\omega \tag{9}$$

At high M_∞, the equations of Ref. 14 indicate an almost constant ratio between the radius of curvature of the shock and body tip, such that $a \cong 1.5b$. This result holds for $M_\infty > 4$ for air. It appears to agree with experiment and to be nearly independent of γ and real gas effects.

A shadowgraph of a blunted cone fired into a ballistics range is shown in Fig. 5. Although the shock cannot be seen near the nose, it can be located relative to the model by measuring from the base. A few points measured from Fig. 5 are compared on Fig. 6 with a hyperbola given by Eq. (9) with $a = 1.5b$. The agreement is at first excellent, but the experimental points fall somewhat below the hyperbola at large values of r_s/b. At still larger values of r_s/b, experiment would again approach the hyperbola. This behavior of the shock is due to an increase in the effective size and a decrease in the effective cone angle near the nose of the model. These changes are associated with the streamline pattern in the flow, which has been expanded around the nose to low density after passing through the shock.

Making use of assumptions of a perfect gas and adiabatic flow outside the boundary layer, Eqs. (8) and (9) can be combined to yield

$$\frac{P_\infty}{P_1}\frac{M_\infty}{M_1}\left(\frac{2 + (\gamma - 1)M_\infty^2}{2 + (\gamma - 1)M_1^2}\right)^{1/2}\left(\frac{a^2}{\tan^2\omega_s - \tan^2\omega}\right) = 2r\theta\left(\frac{\delta}{\theta} - H\right) \tag{10}$$

Expansion of the Flow Behind the Bow Shock

A second relation between M_1 and ω_s can be derived by assuming isentropic flow along each streamline from the bow shock to the outer edge of the boundary layer. This assumption and the oblique shock equations for a perfect gas yield the following equation:

$$\left(\frac{P_1}{P_\infty}\right)^{(\gamma-1)/\gamma}\left[1 + \frac{\gamma - 1}{2}M_1^2\right] = \left[\frac{\gamma + 1}{2\gamma M_\infty^2 \sin^2\omega_s - (\gamma - 1)}\right]^{1/\gamma} \times \left\{\frac{(\gamma + 1)M_\infty^2 \sin^2\omega_s[2 + (\gamma - 1)M_\infty^2]}{2[2 + (\gamma - 1)M_\infty^2 \sin^2\omega_s]}\right\} \tag{11}$$

Calculation of the Mach Number Gradient

An expression for dM_1/dx can be obtained from Eqs. (10) and (11). Although these equations do not require P_1 =

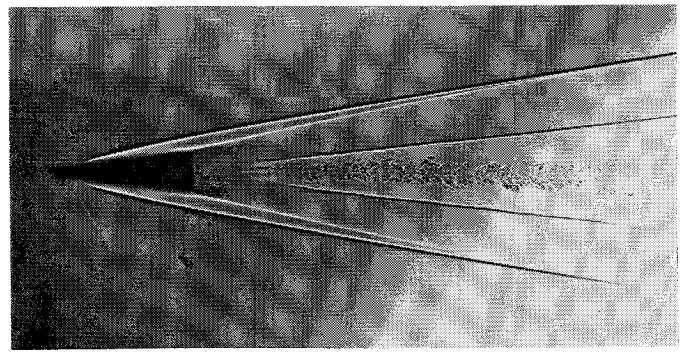

Fig. 5 Shadowgraph, Naval Ordnance Laboratory ballistics range, $M_\infty = 7.63$, $\sigma = 6.33°$.

const, this assumption will now be used. Differentiation with respect to x, use of Eq. (7), and elimination of $d\omega_s/dx$ gives

$$\frac{2\theta}{M_1[2 + (\gamma - 1)M_1^2]} \left\{ \frac{[2 + (\gamma - 1)M_1^2] - 6.41}{F_1} \right\} \times \frac{dM_1}{dx} = \frac{d\theta}{dx} + \frac{\theta}{r}\frac{dr}{dx} \quad (12)$$

where

$$F_1 = \{2 + (\gamma - 1)M_1^2 - 6.41\} \Big/ \left\{ \frac{M_1^2 \tan^2\omega_s \sec^2\omega_s}{2\ (\tan^2\omega_s - \tan^2\omega)} \times \frac{[2\gamma M_\infty^2 \sin^2\omega_s - (\gamma - 1)][2 + (\gamma - 1)M_\infty^2 \sin^2\omega_s]}{(M_\infty^2 \sin\omega_s - 1)^2} - [1 - (\gamma - 1)M_1^2] \right\} \quad (13)$$

Integration of the Momentum Equation

With dM_1/dx given by Eq. (12), Eq. (2) can be written in the following form:

$$\frac{d\theta}{dx} + \frac{\theta}{r}\frac{dr}{dx} = \frac{c_f}{2}\left(\frac{1}{1 + F_1}\right) \quad (14)$$

For $F_1 = 0$, this reduces to the momentum equation for an axisymmetric body with zero pressure gradient and isentropic flow outside the boundary layer. For the conical portion of the blunted cone, $dr/dx = r/x$. With this relation and Eq. (3), Eq. (14) can be written

$$2(R_{\theta c}/R_c)[d(R_c R_{\theta c})/dR_c] = F_2 \quad (15)$$

where

$$F_2 = \frac{0.441}{1 + F_1}\frac{\rho_c u_c}{\rho_1 u_1}\frac{\mu_1}{\mu_c}\frac{T_1}{T'}\frac{\mu'}{\mu_1} \quad (16)$$

and

$$\rho_c u_c/\rho_1 u_1 = (M_c/M_1)(T_1/T_c)^{1/2} \quad (17)$$

$$T_1/T_c = [2 + (\gamma - 1)M_c^2]/[2 + (\gamma - 1)M_1^2] \quad (18)$$

The values of x and θ in the Reynolds numbers R_c and $R_{\theta c}$ are for the blunted cone. The subscript c denotes flow conditions on a sharp cone. These conditions exist on the blunted cone far from the tip.

Starting the integration at the tangent point of the spherical segment and conical section, Eq. (15) becomes

$$\frac{1}{3}(R_c^3 - R_{cn}^3) \int_{(R_c R_{\theta c})_n}^{R_c R_{\theta c}} \frac{2}{F_2}(R_c R_{\theta c})d(R_c R_{c\theta}) \quad (19)$$

where the subscript n denotes values at the tangent point. Dividing both sides by R_{bc}^4 and defining $\xi = R_c R_{\theta c}/R_{bc}^2$,

$$\frac{(R_c/R_{bc})^3 - \cot^3\sigma}{3R_{bc}} = \int_{\xi_n}^{\xi} \frac{2}{F_2}\xi d\xi \quad (20)$$

Equation (20) is a convenient form to integrate. Given the flight conditions, cone angle, and surface temperature, the parameters F_2 and ξ under the integral are functions of only M_1 and ω_s. The parameter F_2 is given by Eq. (16). Combining Eqs. (7) and (10), using $a = 1.5b$, and noting that $r/x = \sin\sigma$,

$$\xi = \frac{\left[\dfrac{0.1755}{\sin\sigma}\dfrac{P_\infty}{P_1}\dfrac{M_\infty}{M_1}\left(\dfrac{2 + (\gamma - 1)M_\infty^2}{2 + (\gamma - 1)M_1^2}\right)^{1/2}\right]}{(\tan^2\omega_s \tan^2\omega)} \quad (21)$$

The integral in Eq. (20) can be evaluated numerically using (Eq. 11) to compute M_1 as a function of ω_s, where ω_s ranges from $\pi/2$ on the axis to ω, the wave angle for a sharp cone (pairs of ω_s and M_1 are used to compute values of F_2 and ξ). It is of interest to note that, except near the nose, Eq. (20) can be written

$$\frac{R_c/R_{bc}}{R_c^{1/4}} \cong \left\{3\int_0^{\xi} \frac{2}{F_2}\xi d\xi\right\}^{1/4}$$

The similarity parameter $(R_c/R_{bc})/R_c^{1/4}$ is equivalent to that given in Ref. 7. Equation (21) shows that R_{bc} does not appear in the calculation of ξ; the value of R_{bc} is needed only in the lower limit ξ_n, which can be obtained by integrating the boundary-layer momentum equation over the spherical segment at the nose. For cases of interest here, the entropy outside the nose boundary layer can be assumed to be constant and equal to the entropy behind the normal shock. Given the flight conditions, cone angle, and surface temperature, the results of Ref. 12 can be used to show that $\xi_n R_{bc}^{1/2} =$ const. Now with a given value of R_{bc} and Eq. (21), Eq. (20) can be used to compute $R_{\theta c}$ vs R_c. Results for additional values of R_{bc} are obtained easily because the parameters under the integral in Eq. (20) will be unchanged, and its evaluation merely starts at a different ξ_n for each R_{bc}.

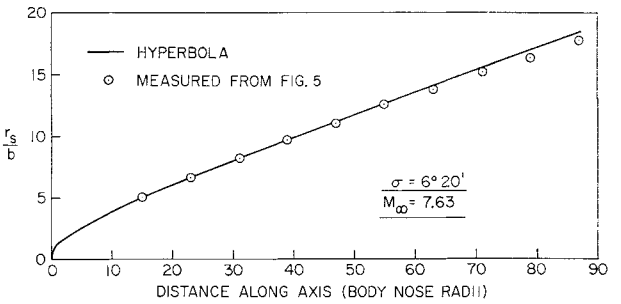

Fig. 6 Comparison of hyperbola and experimental shock shape.

Having values of $R_{\theta c}$, the momentum-thickness Reynolds number based on local flow conditions is

$$R_{\theta 1} = (\rho_1 u_1/\rho_c u_c)(\mu_c/\mu_1)R_{\theta c} \quad (22)$$

For a sharp cone $T_1 = T_c$, and

$$F_2 = F_2^0 = 0.441 T_c \mu'/T'\mu_c = \text{const} \quad (23)$$

The boundary-layer growth over the sharp cone from Eq. (19) is

$$R_{\theta c}^0 = (F_2^0 R_c/3)^{1/2} \quad (24)$$

Friction and Heat Transfer

After integrating the momentum equation for the blunted cone, local values of skin-friction coefficient c_f are given by Eqs. (3) and (22). For comparison with sharp-cone results, it is convenient to define a blunt-cone skin-friction coefficient

$$c_{fc} = 2\tau_w/\rho_c u_c^2 = (M_1^2/M_c^2)c_f \quad (25)$$

The local friction coefficient on a sharp cone is obtained by rewriting Eq. (3)

$$c_{fc}^0 = 0.441\ T_c\mu'/T'\mu_c R_{\theta c}^0 \quad (26)$$

where $R_{\theta c}^0$ is given by Eq. (24). Since c_{f_c} and $c_{f_c}^0$ are based on the same flow conditions, a comparison will show the effect of blunting on local shear stress.

The effect of blunting on heat transfer is not identical to the effect on shear stress. The local heat-transfer rates on the blunt and sharp cones are given by

$$q = \rho_1 u_1 St(T_{e1} - T_w) \qquad q^0 = \rho_c u_c St_c^0(T_{ec} - T_w) \quad (27)$$

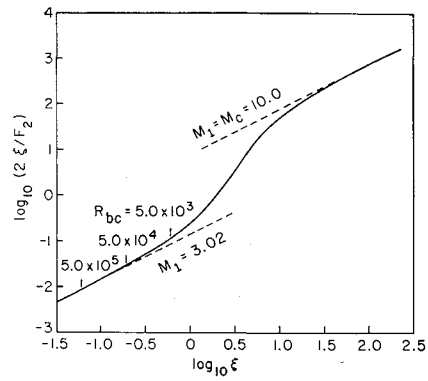

Fig. 7 Numerical values of $2\xi/F_2$, $M_\infty = 14.9$, $M_c = 10.0$, $\sigma = 8°$, $T_\infty = T_w = 530°R$.

Assuming that the flat-plate Reynolds analogy $St = c_f/2Pr^{2/3}$ applies in each case, then

$$\frac{q}{q^0} = \frac{M_c}{M_1}\left(\frac{T_c}{T_1}\right)^{1/2}\left(\frac{T_{e1} - T_w}{T_{ec} - T_w}\right)\left(\frac{c_{fc}}{c_{fc}{}^0}\right) \tag{28}$$

where

$$T_e \equiv T\{1 + Pr^{1/2}[(\gamma - 1)/2]M^2\}$$

For given M_c and T_w/T_c, the ratio of q/q^0 to $c_{fc}/c_{fc}{}^0$ is a function only of M_1.

Local Flow Conditions Far From the Tip

Far from the tip, $R_{\theta c}$ and $R_{\theta 1}$ both approach $R_{\theta c}{}^0$. A numerical example that follows shows that $R_{\theta 1}$ approaches $R_{\theta c}{}^0$ faster than does $R_{\theta c}$. Therefore, substituting in Eq. (22) the value of $R_{\theta c}{}^0$ from Eq. (24) for $R_{\theta 1}$ far from the tip gives the value of $R_{\theta c}$ for the blunt cone:

$$R_{\theta c} \cong \rho_c u_c \mu_1 (F_2{}^0 R_c/3)^{1/2}/\rho_1 u_1 \mu_c$$

This can be rewritten

$$R_c/R_{bc}{}^{4/3} \cong [\rho_1 u_1 \mu_c \xi (3/F_2{}^0)^{1/2}/\rho_c u_c \mu_1]^{2/3} \tag{29}$$

For given flight conditions, cone angle, and surface temperature, $R_c/R_{bc}{}^{4/3}$ given by Eq. (29) is a function of M_1 only. If a value of M_1 (less than M_c) is chosen to define a point on the cone at which the boundary layer has swallowed the variable entropy layer, Eq. (29) shows that the swallowing distance is proportional to the $\frac{4}{3}$ root of the tip radius.

Real Gas Effects

Although a thermally and calorifically perfect gas has been considered here, real gas data for equilibrium air can be introduced in a straightforward way. Reference 15 presents a method for doing this for the calculations of Zakkay and Krause. For the present work, the inviscid solution to the conical flow over a sharp cone in equilibrium air is required. This will give the pressure for the blunt cone, the asymptotic value of bow shock angle and flow conditions at the edge of the boundary layer far from the tip. Equation (1) holds for the real gas case. However, when the perfect gas assumption is removed, Eq. (2) must be rewritten

$$\frac{d\theta}{dx} + \frac{2\theta}{u_1}\left(1 + \frac{u_1}{2\rho_1}\frac{d\rho_1}{du_1} - \frac{[(\delta/\theta) - H]}{2}\right)\frac{du_1}{dx} + \frac{\theta}{r}\frac{dr}{dx} = \frac{c_f}{2} \tag{30}$$

The density ρ_1 and velocity u_1 mentioned previously are related by the constant pressure and adiabatic flow assumptions. The T' (reference temperature) method for calculating c_f, Eq. (3), must be replaced by the reference enthalpy method.[10] It is suggested that the values of δ/θ and H be computed from Eqs. (5) and (6) after replacing T'/T_1 by ρ_1/ρ'. The result given by Eq. (7) will be unchanged. Equation (10), which resulted from continuity considerations, must be replaced by

$$\frac{\rho_\infty u_\infty}{\rho_1 u_1}\left(\frac{a^2}{\tan^2\omega_s - \tan^2\omega}\right) = 2r\theta[(\delta/\theta) - H] \tag{31}$$

Differentiating Eq. (31) with respect to x and combining the result with Eq. (30) yields an integral equation in the same form as Eq. (20). A second relation between u_1 and ω_s is necessary to compute the boundary-layer growth. This relation can be obtained in the same manner as Eq. (11), but, using real gas data, an analytic result cannot be given.

Numerical Example

Numerical results are presented for the case $\sigma = 8°$, $M_\infty = 14.9$, and $T_\infty = T_w = \text{const} = 530\ °R$ (corresponding to the early flight of a heat-sink model fired into a ballistics range) for $R_{bc} = 5.0 \times 10^3$, 5.0×10^4, and 5.0×10^5. With $M_\infty = 14.9$, the local Mach number on a sharp cone is $M_c = 10.0$. For inviscid flow, the Mach number on the blunted cone is $M_1 = 3.02$, corresponding to the flow that has passed through the normal portion of the bow shock.

The integrand of the integral in Eq. (20) is plotted vs the variable of integration on Fig. 7. First note that Eq. (13) gives $F_1 = 0$ for $\omega_s = \pi/2$ and $\omega_s = \omega$. For the present case, F_1 reached a maximum value of 0.6 at $\omega_s \cong 30°$. It is of interest to point out that during the swallowing process F_1, and thus the Mach number gradient dM_1/dx, has a significant effect on the rate of boundary-layer growth. This can be seen from Eq. (14). Near the nose F_2, given by Eq. (16), can be approximated by taking $M_1 = 3.02$ and $F_1 = 0$. Far from the nose F_2 can be approximated by taking $M_1 =$

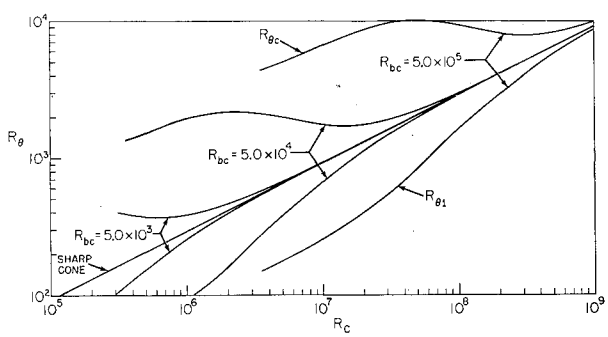

Fig. 8 Effect of bluntness on momentum-thickness Reynolds number, $M_\infty = 14.9$, $M_c = 10.0$, $\sigma = 8°$, $T_\infty = T_w = 530°R$.

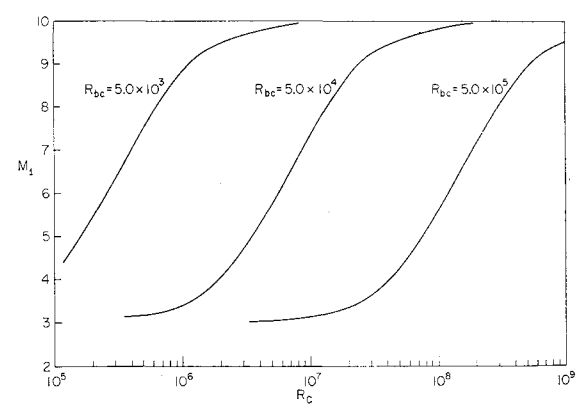

Fig. 9 Effect of bluntness on local Mach number, $M_\infty = 14.9$, $M_c = 10.0$, $\sigma = 8°$, $T_\infty = T_w = 530°R$.

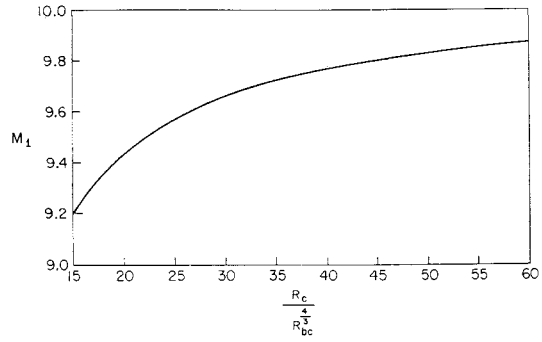

Fig. 10 Effect of Reynolds number on local Mach number, $M_\infty = 14.9$, $M_c = 10.0$, $\sigma = 8°$, $T_\infty = T_w = 530°R$.

10.0 and $F_1 = 0$. Each of these limiting values of F_2 gives a straight line on Fig. 7. Figure 7 indicates that there can be three flow regimes. Near the nose the Mach number and entropy outside the boundary layer can be almost constant and correspond to the flow through the normal portion of the shock. Next there is a regime in which the boundary layer "swallows" the variable entropy layer and the Mach number and entropy are changing. Finally, far from the nose the Mach number and entropy are again almost constant and correspond to the flow through the conical portion of the shock.

It is necessary to obtain lower limits in order to evaluate the integral in Eq. (20). A modified Newtonian pressure distribution was assumed and the boundary-layer growth over the nose calculated by the method of Ref. 12. The result is $\xi_n = 43/R_{bc}^{1/2}$. The lower limits for each of the three nose Reynolds numbers are indicated on Fig. 7. The portion of the variable entropy layer swallowed by the nose boundary layer is small in all cases. The assumption of normal shock entropy was made for the flow over the nose and is therefore justified. The effects of errors in the lower limits quickly become negligible as the boundary layer grows along the conical section.

Curves of $R_{\theta c}$ vs R_c from Eq. (20) are shown on Fig. 8. The sharp-cone curve was obtained from Eq. (24). Since the $R_{\theta c}$ values are based on sharp-cone flow conditions, comparison with sharp-cone results shows the effect of bluntness on θ. Blunt-cone values can be greater by an order of magnitude. Curves of $R_{\theta 1}$ from Eq. (22) are also plotted on Fig. 8. The values are always below the sharp-cone curve. Thus, despite the increase in θ, bluntness reduces the momentum-thickness Reynolds number based on local flow conditions.

Curves of M_1 vs R_c generated in solving Eq. (20) are plotted in Fig. 9. They show that bluntness affects the local Mach number far from the nose. This means that, for a cone of finite length, the bluntness ratio (ratio of nose to base radius) must be very small before $M_1 = M_c$ near the base. As an example, take $R_{bc} = 5.0 \times 10^3$. Figure 9

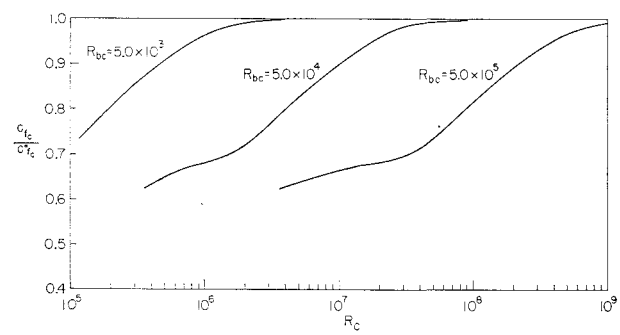

Fig. 11 Effect of bluntness on local skin-friction coefficient, $M_\infty = 14.9$, $M_c = 10.0$, $\sigma = 8°$, $T_\infty = T_w = 530°R$.

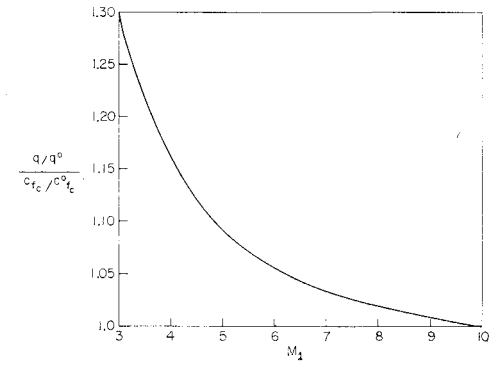

Fig. 12 Comparison of heat-transfer and skin-friction ratios, $M_\infty = 14.9$, $M_c = 10.0$, $\sigma = 8°$, $T_\infty = T_w = 530°R$.

shows that $M_1 \cong M_c = 10$ when $R_c = 10^7$. The bluntness-ratio, given by $R_{bc}/R_c \sin\sigma$, for this case is only 0.0036.

Equation (29) was derived to show that, far from the nose, the relation between M_1 and $R_c/R_{bc}^{4/3}$ can be obtained without integrating the momentum equation. One curve serves for all values of R_{bc} (Fig. 10).

Values c_{f_c} and $c_{f_c}^0$ were computed from Eqs. (25) and (26), respectively. The ratio is plotted in Fig. 11 vs R_c. The curves show that bluntness significantly reduces the local shear stress. For a slender cone, a large fraction of the total drag is due to friction. A slight bluntness will therefore measurably decrease the total drag. This method for computing skin friction was used in the calculations of total drag made in Ref. 16. Excellent agreement was obtained with ballistic-range measurements.

Bluntness will also reduce heat-transfer rate. However, the reduction is smaller than for friction. The comparison of the effect on heat transfer to the effect on friction given by Eq. (28) is shown as a function of M_1 in Fig. 12. At M_1 near 3, Fig. 12 shows that q/q^0 is 30% greater than $c_{f_c}/c_{f_c}^0$. This is in the neighborhood of the tangent point where $c_{f_c}/c_{f_c}^0 = 0.6$.

The results of the numerical example just discussed can be used to verify one of the assumptions made in the analysis, $\tau_1/\rho_1 u_1^2 \ll c_f/2$. Now

$$\frac{\tau_1/\rho_1 u_1^2}{c_f/2} = \frac{\tau_1}{\tau_w} = \frac{\mu_1 (du/dy)_{u=u_1}}{\tau_w}$$

The value of $(du/dy)_{u=u_1}$ can be obtained from du_1/dx using continuity considerations. A maximum value of $\tau_1/\tau_w = 0.036$ occurred during the swallowing process and is inde-

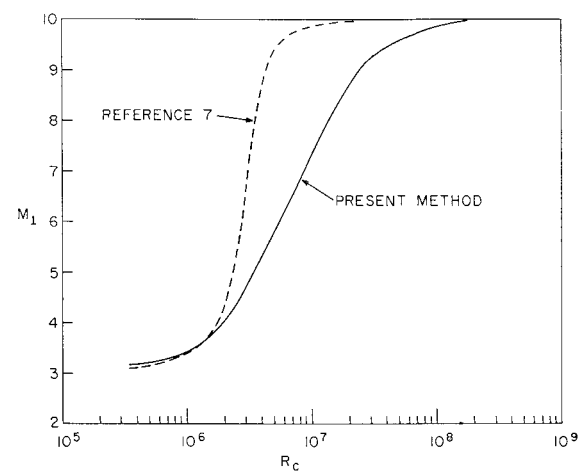

Fig. 13 Comparison of methods, $M_\infty = 14.9$, $M_c = 10.0$, $\sigma = 8°$, $T_\infty = T_w = 530°$ R, $R_{bc} = 5.0 \times 10^4$.

pendent of the nose radius. The assumption that τ_1 can be neglected is thus justified for the numerical example.

The method given here for calculating M_1 is compared in Fig. 13 with that given in Ref. 7. To make a meaningful comparison, the edge of the boundary layer was taken at $u/u_1 = 0.995$, and the same shock shape (hyperbola) was assumed for both cases. Although the agreement is reasonable at low values of M_1, the results diverge during the swallowing process. The values of R_c at which the swallowing is essentially complete differ by an order of magnitude. Experimental values of M_1 on a slender cone at a high M_∞ would be useful in resolving this difference.

References

[1] Brinich, P. F. and Diaconis, N. S., "Boundary-layer development and skin friction at Mach number 3.05," NACA TN 2742 (1952).

[2] Brinich, P. F., "Effect of leading edge geometry on boundary-layer transition at Mach 3.1," NACA TN 3659 (1956).

[3] Brinich, P. F. and Sands, N., "Effect of bluntness on transition for a cone and a hollow cylinder at Mach 3.1," NACA TN 3979 (1957).

[4] Rogers, R. H., "The effect of tip bluntness on boundary-layer transition on a 15° included angle cone at M = 3.12 and 3.81," Royal Aircraft Establishment TN Aero. 2645 (1959).

[5] Brinich, P. F., "Recovery temperature, transition, and heat-transfer measurements at Mach 5," NASA TN D-1047 (1961).

[6] Moeckel, W. E., "Some effects of bluntness on boundary-layer transition and heat transfer at supersonic speeds," NACA TR 1312 (1957); supersedes NACA TN 3653 (1956).

[7] Zakkay, V. and Krause, E., "Boundary conditions at the outer edge of the boundary layer on blunted conical bodies," Aeronautical Research Lab. 62-386 (1962); also AIAA J. **1**, 1671–1672 (1963).

[8] Lees, L., "Laminar heat transfer over blunt-nosed bodies at hypersonic flight speeds," Jet Propulsion **26**, 259–269 (1956).

[9] Rubesin, M. W. and Johnson, H. A., "A critical review of skin-friction and heat-transfer solutions of the laminar boundary layer of a flat plate," Trans. Am. Soc. Mech. Engrs. **71**, 383–388 (1949).

[10] Wilson, R. E., "Real-gas laminar boundary-layer skin friction and heat transfer," J. Aerospace Sci. **29**, 640–647 (1962).

[11] Van Driest, E. R., "Investigation of laminar boundary layer in compressible fluids using the Crocco method," NACA TN 2597 (1952).

[12] Cohen, C. B. and Reshotko, E., "The compressible laminar boundary layer with heat transfer and arbitrary pressure gradient," NACA TR 1294 (1956).

[13] Moeckel, W. E., "Approximate method for predicting form and location of detached shock waves ahead of plane or axially symmetric bodies," NACA TN 1921 (1949).

[14] Heybey, W. H., "Shock distances in front of symmetrical bodies," Naval Ordnance Lab., Naval Ordnance Test Station, Rept. NavOrd 3594 (1953).

[15] Rubin, I., "Shock curvature effect on the outer edge conditions of a laminar boundary layer," AIAA J. **1**, 2850–2852 (1963).

[16] Lyons, W. C., Jr., Brady, J. J., and Levensteins, Z. J., "Hypersonic drag, stability, and wake data for cones and spheres," AIAA Preprint 64-44 (1964).